

Sisyphus Optical Lattice Decelerator

Chun-Chia Chen (陳俊嘉), Shayne Bennetts, Rodrigo González Escudero, Florian Schreck, Benjamin Pasquiou*
*Van der Waals-Zeeman Institute, Institute of Physics, University of Amsterdam,
 Science Park 904, 1098XH Amsterdam, The Netherlands*
 (Dated: December 15, 2024)

We experimentally demonstrate a variation on a Sisyphus cooling technique that was proposed for cooling antihydrogen. In our implementation, atoms are selectively excited to an electronic state whose energy is spatially modulated by an optical lattice, and the ensuing spontaneous decay completes one Sisyphus cooling cycle. We characterize the cooling efficiency of this technique on a continuous beam of Sr, and compare it with the case of a Zeeman slower. We demonstrate that this technique provides similar atom number for lower end temperatures, provides additional cooling per scattering event and is compatible with other laser cooling methods.

The asymmetry between matter and antimatter is one of the great mysteries of modern physics. A promising avenue to better understand this asymmetry is to precisely compare spectra of hydrogen with antihydrogen, but this requires the ability to generate robust trapped samples of ultracold antihydrogen [1–5]. Unlike hydrogen, anti-hydrogen can not be cooled through evaporation [6], a cooling method relying on thermalization by interparticle collisions. Since anti-hydrogen atoms are produced in such small numbers collisions are rare and the thermalization rates are impractical for evaporation [1, 2]. Instead, laser cooling is needed at 121.6 nm where performances remain strongly constrained by current laser technology despite heroic efforts [7–9]. The proposal in Wu *et al.* [10] overcomes these limitations by allowing the extraction of many photon recoils of momentum per scattering event by the simple addition of an optical lattice.

This technique is not limited to cooling anti-hydrogen. Most molecules lack closed cycling transitions and thus this cooling technique can improve performance by dramatically increasing the energy extracted per scattering event. This provides opportunities to continue the recent rapid advancements in the cooling and trapping of complicated many-atom systems such as molecules [11–16]. In turn, progress in molecule cooling is opening a plethora of ways to probe new physics with impacts at the very foundations of physics [17, 18]. Some of the most prominent include tests for the possible variation of fundamental constants [19] and tests of the validity of fundamental symmetries [20–25].

A range of approaches have been devised to achieve improved performance while relaxing constraints imposed by traditional Doppler cooling techniques. For example, rapid cycling using stimulated emission can provide stronger momentum transfer without spontaneous heating or loss from non closed cycling transitions. This is demonstrated in bichromatic force cooling [26], adiabatic rapid passage [27] and SWAP cooling [28] but it requires intense resonant light not available at the 121.6 nm transition needed for anti-hydrogen. Alternatively, Sisyphus-like cooling methods [29], where kinetic energy is converted into potential energy, can function

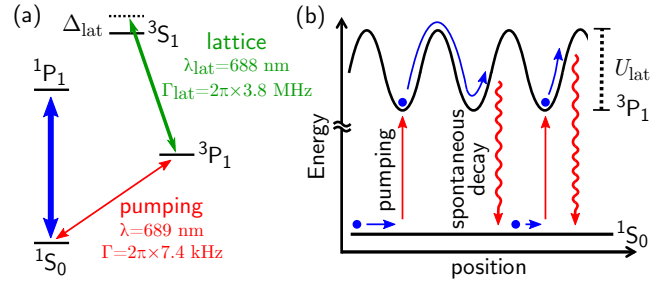


Figure 1. (a) Relevant electronic levels of strontium and the two transitions used for pumping and optical lattice creation, which are both necessary for the Sisyphus Optical Lattice Decelerator. (b) Schematic of two typical cooling cycles, from pumping to spontaneous decay.

effectively even at very low pumping rates and are routinely applied to beat the Doppler temperature limit [30]. Examples of this approach include Zeeman Sisyphus decelerators [31] and Rydberg-Stark decelerators [32, 33] where a photon excitation changes the internal state allowing a significant part of the slowing to be done by an externally applied electromagnetic field gradient.

In this article, we present a proof-of-principle demonstration of a variation on the scheme proposed by Wu *et al.* [10] to laser cool antihydrogen. Without using radiation pressure, we slow a continuous stream of strontium atoms using a Sisyphus-like deceleration mechanism also described in other proposals [34–36]. The method uses a 1D optical lattice acting on the excited $3P_1$ electronic state combined with a selective pumping mechanism that excites atoms to the lattice potential minima. We explore the performance of this technique, which we name a Sisyphus Optical Lattice Decelerator (SOLD), for various atomic beam velocities and lattice heights. Compared with the standard Zeeman slower (ZS) we show that the SOLD obtains similar fluxes but with lower temperatures and zero mean final velocity. In principle, by using a deep lattice very few pumping photons can be sufficient to bring fast atoms to rest, making SOLD a good decelerator candidate for exotic species and molecules without a closed cycling transition.

The working principle of the SOLD relies on a 3-level

system coupled by two optical transitions, something ubiquitous for both atomic and molecular species. Our implementation using strontium is depicted in Fig. 1(a). An optical lattice is formed using a pair of coherent counter-propagating beams with a frequency in the vicinity of the $^3P_1 - ^3S_1$ transition. This produces a spatially modulated coupling between the 3P_1 and 3S_1 states and thus a spatially modulated light shift on the excited 3P_1 state. The ground 1S_0 state remains essentially unaffected. By applying a laser resonant with the $^1S_0 - ^3P_1$ transition atoms can be optically pumped into the 3P_1 state where they experience the force associated with the lattice potential, see Fig. 1(b). If the linewidth Γ of the narrow 7.4 kHz $^1S_0 - ^3P_1$ intercombination line is much smaller than the lattice height $U_{\text{lat}} \gg \hbar\Gamma$, this “pumping” laser can be tuned to selectively address the bottom of the lattice sites. Atoms pumped into 3P_1 will then climb up the lattice potential hills and lose kinetic energy before spontaneously decaying back to the ground state as shown in Fig. 1(b). As atoms in 1S_0 continue to propagate along the lattice axis, this cooling cycle can repeat like a Sisyphus mechanism. By making the lattice very deep it is theoretically possible to remove most of the forward kinetic energy of an atom with a single cycle, as in Rydberg-Stark decelerators [32, 33], and potentially within distances on the order of the lattice period. The theoretical temperature limit for this scheme is the higher of an effective Doppler temperature depending on Γ [35], or the recoil temperature associated with spontaneous emission.

To demonstrate experimentally the feasibility of the SOLD, we implement the setup shown in Fig. 2(a). We start with a magneto-optical trap (MOT) operating in a steady-state regime on the narrow 7.4 kHz $^1S_0 - ^3P_1$ inter-combination line, as described in our previous work (configuration “Red MOT I” of [37]). We overlap this MOT with an optical dipole trap acting as a “transport” guide [38]. This 1D guide is $\sim 35 \mu\text{K}$ deep at the MOT location and propagates horizontally along the z axis. By adding a “launch” beam resonant with the $^1S_0 - ^3P_1$ π transition and pointed at the overlap between the MOT and transport guide, we outcouple MOT atoms into the guide with a well-controlled mean velocity ranging from 0.08 to 0.25 m.s $^{-1}$ [39]. Atoms then propagate along the transport guide for ~ 3.7 cm until they reach the decelerator region.

We produce a 1D lattice potential with a pair of counter-propagating laser beams whose frequency is blue-detuned by $\Delta_{\text{lat}} \approx 30$ GHz from the $^3P_1 - ^3S_1$ transition. The lattice beams cross the transport guide at a shallow angle of 6° , overlapping the atomic beam for about 3.4 mm. Optical “pumping” from the 1S_0 to 3P_1 state is provided by illuminating the atoms from the radial direction. Pumping laser beams are 15 kHz red detuned from the π transition and their combined intensity corresponds to a saturation parameter of ~ 1 . In addition to pumping, these beams provide an optical mo-

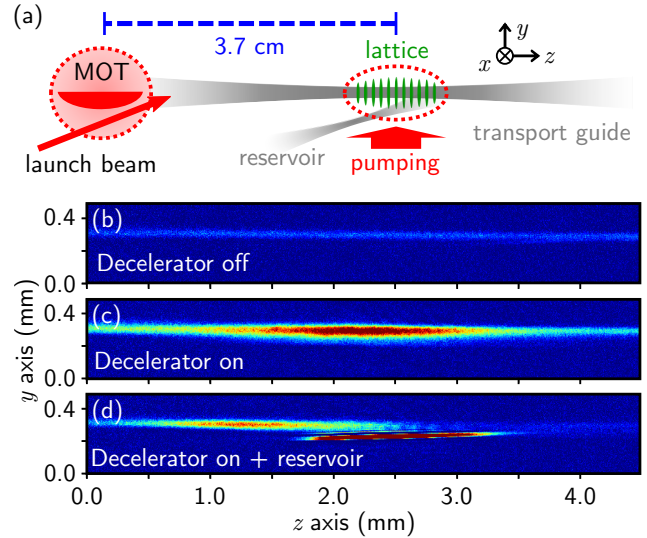


Figure 2. (a) Side view of the setup. (b,c,d) Absorption imaging pictures of the atomic beam at the location of the decelerator, (b) without lattice, (c) with lattice, and (d) with both lattice and reservoir trap.

lasses effect, which brings the atoms’ radial temperature to $\sim 2 \mu\text{K}$. Importantly, there is no near-resonant light capable of slowing atoms in the z axis in the absence of the SOLD optical lattice.

We operate the decelerator on a guided atomic beam continuously fed by the MOT, with a homogeneous axial density across the full 4.5 mm of the field of view of our imaging region, see Fig. 2(b). When the lattice is switched on, the density in the overlap region between the atomic and lattice beams sharply increases, suggesting an accumulation of slowed atoms, as shown in Fig. 2(c). Without either lattice beam or with a large (160 MHz) frequency difference between the two lattice beams, this feature vanishes. Fig. 2(c) also shows that some atoms travel completely across the lattice region due to incomplete slowing or diffusion from the lattice region. Note that our slowing mechanism is fully compatible with a steady-state apparatus, and we perform our measurements after reaching steady state.

For better characterization of the SOLD, and since we are concerned about diffusion of slowed atoms, we add a second “reservoir” dipole trap beam. This beam crosses below the transport guide at the lattice location, with an offset adjusted to allow slow atoms to pass from the guide into the reservoir while not seriously disturbing the potential landscape of the guide itself. Thus, the reservoir collects and stores slowed atoms 2 mm away from the crossing, see Fig. 2(a). We measure the mean velocity selectivity of the loading of this reservoir [39], which matches a Gaussian centered around zero velocity with a width of $\sigma_v = 0.0084(4) \text{ m.s}^{-1}$. We show one example of loading into this reservoir in Fig. 2(d), which also exemplifies a means of atom extraction from our ultracold atom source. We show in Fig. 3 the measured

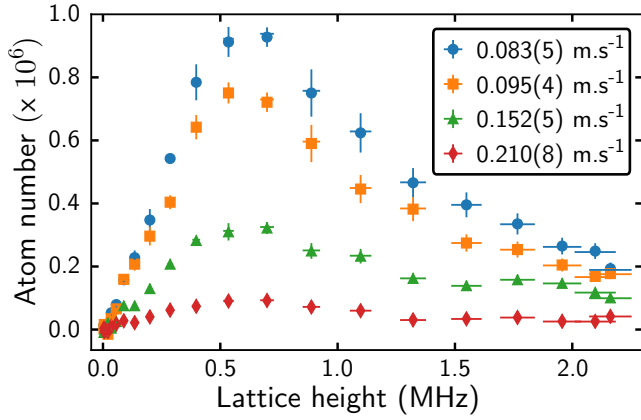


Figure 3. Performances of the SOLD for several beam mean velocities. The measured steady-state number of atoms loaded in the reservoir is shown for varying lattice height. The four data sets represent four different incoming velocities before the lattice region. The vertical error bars represents standard errors from binned data points. The horizontal error bars origin is described in [39].

atom number loaded into the reservoir by the SOLD, depending on the lattice height and for various beam velocities. The efficiency is poor for small lattices, as not enough kinetic energy is removed before atoms leave the lattice location. For increasing lattice height, we observe a clear loading optimum, followed by a slow decrease. These two features originate from the pumping rate to 3P_1 , which depends on both lattice height and velocity.

We can better understand the SOLD slowing efficiency using a simple semi-classical model. Consider an atom initially pumped into the 3P_1 state at the bottom of the lattice potential $U_{\text{lat}} \sin^2(k_{\text{lat}}z)$. U_{lat} is the lattice height and $k_{\text{lat}} = 2\pi/\lambda_{\text{lat}}$ is the lattice wavevector, oriented along the z axis. In Fig. 4(a), we plot the dependence of the average energy lost per pump cycle E_{lost} with incoming velocity v and lattice height. For high kinetic energies compared to the lattice height $\frac{1}{2}mv^2 \gg U_{\text{lat}}$, the energy E_{lost} saturates. In this case, atoms travel through several lattice sites, and lose $E_{\text{lost}} \approx \frac{U_{\text{lat}}}{2} / \left(1 + (\Gamma/2k_{\text{lat}}v)^2\right)$ [39]. For our experimental conditions $v \gg \lambda_{\text{lat}}\Gamma$, E_{lost} saturates to $U_{\text{lat}}/2$. A striking feature of Fig. 4(a) is that E_{lost} exhibits a sharp resonance for $\frac{1}{2}mv^2 = U_{\text{lat}}$, where cooling is the most efficient. In this case, atoms have just enough energy to climb to the top of the first lattice hill where they spend most of their time and are thus more likely to undergo spontaneous emission. They therefore lose a maximum energy, which asymptotically reaches $E_{\text{lost}} \rightarrow U_{\text{lat}}$ for $v \gg \lambda_{\text{lat}}\Gamma$. In contrast to Ref. [10], which relies also on a spatial modulation of Γ , the effective rate of spontaneous emission in our case is higher on lattice hills only because of the increased time atoms spend there.

An important benchmark for a laser cooling technique is the average number of photons which needs to be scattered to slow atoms from some initial velocity to the

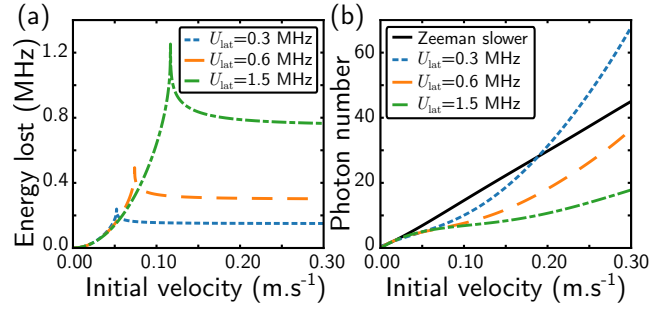


Figure 4. Efficiency of our cooling scheme, depending on lattice height and initial atom velocity. (a) Average energy E_{lost} lost during the first cooling cycle. (b) Number of cycles/pumping photons needed for the SOLD compared with a Zeeman slower, during the cooling process down to a kinetic energy below $2\mu\text{K}$. The plain black line shows the behavior of the ZS, while the dotted, dashed and dash-dotted lines are for the SOLD with lattice heights U_{lat} of 0.3 MHz, 0.6 MHz and 1.5 MHz, respectively.

final velocity allowed by this technique. In Fig. 4(b) we calculate the number of pumping photons needed to reach a kinetic energy equivalent to a temperature below $2\mu\text{K}$. This temperature was arbitrarily chosen ~ 4 times larger than the recoil temperature associated with the $^1S_0 - ^3P_1$ transition, the relevant cooling limit in our case. For comparison we also show a conventional Doppler cooling process, the Zeeman slower (ZS) [40]. Fig. 4(b) shows that, for high initial velocities, a proper choice of the lattice height lead to the SOLD requiring much less cooling photons than the ZS.

The SOLD ability to slow atoms with high incoming velocities is strongly dependent on the pumping rate. We model this rate by solving the optical Bloch equations for a two-level system for varying velocity and lattice height. We consider the ground 1S_0 and excited 3P_1 states coupled by the pumping laser, and numerically solve for the populations with time [39]. For this calculation, we assume a constant velocity, which is valid for $\frac{1}{2}mv^2 \gg U_{\text{lat}}$. After a variable time, the excited state population reaches a steady-state only slightly perturbed by the time-dependent detuning produced by travelling within the lattice. Averaging over this small perturbation, we get the population in the 3P_1 state which we show in Fig. 5(a).

The remarkable feature in Fig. 5(a) is the presence of multiple resonances where there are high pumping rates. These resonances can be explained by in-phase multiple π -over- N pulses. Indeed, only at the bottom of a lattice site is the detuning small enough to pump a significant population to 3P_1 . While the atoms propagate from one site to the next, the 1S_0 and 3P_1 states acquire different phases. Once at the next site, the following pulse efficiently pumps further population to 3P_1 only if the dephasing is equal to multiples of 2π , see Fig. 5(b). This

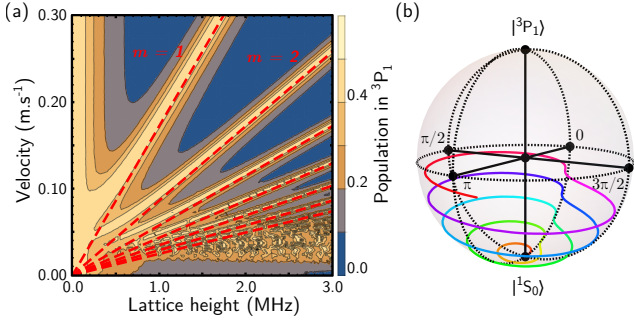


Figure 5. (a) Time-averaged population transferred to the excited 3P_1 state depending on the lattice height and the atom velocity. For clarity of the figure, the population is calculated for a saturation parameter of the pumping $^1S_0 - ^3P_1$ transition of about 1600 instead of the $0.1 \sim 10$ typically used in our setup. The dashed red lines show the condition of eq. (1) for $m \in \{1 \dots 7\}$. (b) Short time evolution of the Bloch vector (for 5 pulses) in the case of in-phase excitation satisfying eq. (1) with $m = 1$.

criterion on the dephasing leads to the relation

$$\frac{U_{\text{lat}}}{h} = m \times \frac{4v}{\lambda_{\text{lat}}}, \quad (1)$$

with $m \in \mathbb{N}$ and h the Planck constant. The maximums in loading efficiency observed in Fig. 3 correspond mainly to the fulfillment of this criterion for the case $m = 1$. Including both the average lost energy E_{lost} and the pumping rate, we model the behavior of the SOLD and reproduce qualitatively the features of the experimental data [39]. Moreover, we find that the criterion of eq. (1) with $m = 1$ dictates the maximum capture velocity of the SOLD, which reads $v_c = U_{\text{lat}} \lambda_{\text{lat}} / 4h$.

We now compare experimentally the SOLD performance with that of a Zeeman slower. To this end, we add a laser beam counter-propagating to the transport guide, focused in the SOLD region and with a circular polarization set to address the $m_J = -1$ Zeeman sub-state. We demonstrated in previous work that it is possible to operate a ZS on the narrow Sr inter-combination line [37]. We report in Tab. I a comparison between the two slowing methods. Both give similar results for fluxes and final atom numbers, with a slight advantage for the ZS, which we attribute mainly to the spatial selectivity of its optical excitation. However, we observe a clear difference in the final axial temperatures T_z within the reservoir, which effectively reflects the final mean velocities. For the SOLD, T_z is almost as low as the radial temperature T_{rad} provided by the molasses cooling, whereas T_z is 2.5 times hotter for the ZS. This is because a Zeeman slower is unable to decelerate atoms to zero velocity, as they remain somewhat resonant with ZS photons and are pushed backwards. On the contrary, for the SOLD the final mean velocity is stationary in the frame of the optical lattice, whose velocity can be set at will by the frequency difference between lattice beams [39, 41, 42].

Table I. Comparison of the SOLD and the Zeeman slower (ZS). The rows give steady-state atoms numbers, fluxes, $1/e$ loading times, and radial (axial) temperatures T_{rad} (T_z). The various configurations are, in order, the SOLD in the transport guide, the SOLD plus the reservoir trap (R), the ZS plus reservoir and the combination of both techniques.

	SOLD	SOLD+R	ZS+R	SOLD+ZS+R
Atom ($\times 10^6$)	0.78(01)	0.69(01)	1.87(04)	2.00(10)
Flux ($\times 10^6 \text{ s}^{-1}$)	0.74(04)	0.65(03)	2.11(14)	2.80(15)
Loading (ms)	705(20)	625(52)	434(43)	507(55)
T_{rad} (μK)		1.53(02)	1.08(04)	1.34(02)
T_z (μK)		2.30(06)	5.67(94)	2.59(10)

An additional difference is that, since the SOLD does not rely on radiation pressure from the pumping beam to cool, it is possible to use a much broader class of transitions than for standard laser cooling methods. It is for example possible to use the ZS beam as a pumping beam that features both spatial and velocity selectivity. The lattice, now acting on atoms in $^3P_1 m_J = -1$, is the one charged with decelerating atoms to zero axial velocity. In presence of both lattice and ZS beams, we observe the best number of atoms captured in the reservoir, while keeping the low temperature T_z due to the SOLD, see Tab. I.

Let us now turn to considerations for further applications of this cooling scheme. Firstly, it is clear from Fig. 5(a) that, at high velocities, pumping rates are low unless the lattice height matches the conditions of eq. (1). This can be dealt with by temporal modulation of the lattice intensity, which varies the resonance locations. Secondly, for lattices much higher than the transport guide depth, we observe a clear spread of the atomic beam out of the guide. This is due both to the radial anti-confinement from the blue-detuned lattice beams and the slight angle between lattice and transport beams. A red-detuned lattice could remedy this by confining the atoms radially, but this will make correctly tuning the pumping frequency dependent on the lattice intensity. Thirdly, if the lattice detuning Δ_{lat} is insufficient, atoms in the 3P_1 state can be optically pumped by the lattice light to 3S_1 [39], where they can decay to the metastable 3P_0 and 3P_2 states, introducing a need for repumping [43]. Lastly, in the applied case proposed by Wu *et al.* [10], the lattice is 78.5 MHz high, and the capture velocity for their scheme is set to $v_{c,H} \approx 25 \text{ m.s}^{-1}$ compared to 13 m.s^{-1} with the SOLD. At this height and velocity $v_{c,H}$, the number of photons required to cool strontium by the SOLD is about 1700, much lower than the ZS case of 3700. Moreover, due to the quadratic shape of the SOLD curve in Fig. 4(b), this number decreases dramatically for incoming lower velocities or for higher lattices. In the case of antihydrogen, it would take about 20 photons for the SOLD alone to cool below 10 mK. Since the scheme of Wu *et al.* also uses the ra-

diation pressure of the pumping photons to slow atoms, applying this scheme to antihydrogen is very appealing.

To summarize, we experimentally demonstrate the feasibility of a Sisyphus-type decelerator first proposed in a slightly different form to laser cool antihydrogen [10, 35, 36]. The efficiency of this decelerator is characterized in the steady-state regime both experimentally and theoretically in dependence of incoming atom velocities and lattice heights. We determine the capture velocity of this technique, and compare the SOLD with a Zeeman slower, where we show axial temperatures a factor of 2.5 lower. With both techniques combined, we profit from both the ZS spatial/velocity selectivity and the SOLD end temperatures. Finally, we briefly consider some improvements and applications to the case of antihydrogen. The SOLD approach requires only selective pumping into a lattice in a three level system, rather than a closed cyclic transition. This could help in the quest to bring new exotic species and molecules to the ultracold regime [12–16]. Moreover, by careful choice of the time sequence for the lattice velocity and intensity a pulsed version of the SOLD could bring an atom wavepacket to any desired velocity while scattering only a handful of photons.

Note added Recently, we became aware of related Sisyphus cooling in optical tweezers [44].

B.P. thanks the NWO for funding through Veni grant No. 680-47-438. We thank the NWO for funding through Vici grant No. 680-47-619 and the European Research Council (ERC) for funding under Project No. 615117 QuantStro. C.-C. C. thanks support from the MOE Technologies Incubation Scholarship from the Taiwan Ministry of Education.

C.-C. C. and S.B. contributed equally to this work.

* SOLD@strontiumBEC.com

- [1] G. B. Andresen, M. D. Ashkezari, M. Baquero-Ruiz, W. Bertsche, P. D. Bowe, E. Butler, C. L. Cesar, S. Chapman, M. Charlton, A. Deller, S. Eriksson, J. Fajans, T. Friesen, M. C. Fujiwara, D. R. Gill, A. Gutierrez, J. S. Hangst, W. N. Hardy, M. E. Hayden, A. J. Humphries, R. Hydomako, M. J. Jenkins, S. Jonsell, L. V. Jørgensen, L. Kurchaninov, N. Madsen, S. Menary, P. Nolan, K. Olchanski, A. Olin, A. Povilus, P. Pusa, F. Robicheaux, E. Sarid, S. Seif el Nasr, D. M. Silveira, C. So, J. W. Storey, R. I. Thompson, D. P. van der Werf, J. S. Wurtele, and Y. Yamazaki, *Nature* **468**, 673 (2010).
- [2] G. Gabrielse, R. Kalra, W. S. Kolthammer, R. McConnell, P. Richerme, D. Grzonka, W. Oelert, T. Seftick, M. Zielinski, D. W. Fitzakerley, M. C. George, E. A. Hessels, C. H. Storry, M. Weel, A. Müllers, and J. Walz (ATRAP Collaboration), *Phys. Rev. Lett.* **108**, 113002 (2012).
- [3] M. Ahmadi, B. X. R. Alves, C. J. Baker, W. Bertsche, E. Butler, A. Capra, C. Carruth, C. L. Cesar, M. Charlton, S. Cohen, R. Collister, S. Eriksson, A. Evans, N. Evetts, J. Fajans, T. Friesen, M. C. Fujiwara, D. R. Gill, A. Gutierrez, J. S. Hangst, W. N. Hardy, M. E. Hayden, C. A. Isaac, A. Ishida, M. A. Johnson, S. A. Jones, S. Jonsell, L. Kurchaninov, N. Madsen, M. Mathers, D. Maxwell, J. T. K. McKenna, S. Menary, J. M. Michan, T. Momose, J. J. Munich, P. Nolan, K. Olchanski, A. Olin, P. Pusa, C. Ø. Rasmussen, F. Robicheaux, R. L. Sacramento, M. Sameed, E. Sarid, D. M. Silveira, S. Stracka, G. Stutter, C. So, T. D. Tharp, J. E. Thompson, R. I. Thompson, D. P. van der Werf, and J. S. Wurtele, *Nature* **541**, 506 (2017).
- [4] M. Ahmadi, B. X. R. Alves, C. J. Baker, W. Bertsche, E. Butler, A. Capra, C. Carruth, C. L. Cesar, M. Charlton, S. Cohen, R. Collister, S. Eriksson, A. Evans, N. Evetts, J. Fajans, T. Friesen, M. C. Fujiwara, D. R. Gill, A. Gutierrez, J. S. Hangst, W. N. Hardy, M. E. Hayden, C. A. Isaac, A. Ishida, M. A. Johnson, S. A. Jones, S. Jonsell, L. Kurchaninov, N. Madsen, M. Mathers, D. Maxwell, J. T. K. McKenna, S. Menary, J. M. Michan, T. Momose, J. J. Munich, P. Nolan, K. Olchanski, A. Olin, P. Pusa, C. Ø. Rasmussen, F. Robicheaux, R. L. Sacramento, M. Sameed, E. Sarid, D. M. Silveira, S. Stracka, G. Stutter, C. So, T. D. Tharp, J. E. Thompson, R. I. Thompson, D. P. van der Werf, and J. S. Wurtele, *Nature* **548**, 66 (2017).
- [5] M. Ahmadi, B. X. R. Alves, C. J. Baker, W. Bertsche, A. Capra, C. Carruth, C. L. Cesar, M. Charlton, S. Cohen, R. Collister, S. Eriksson, A. Evans, N. Evetts, J. Fajans, T. Friesen, M. C. Fujiwara, D. R. Gill, J. S. Hangst, W. N. Hardy, M. E. Hayden, E. D. Hunter, C. A. Isaac, M. A. Johnson, J. M. Jones, S. A. Jones, S. Jonsell, A. Khramov, P. Knapp, L. Kurchaninov, N. Madsen, D. Maxwell, J. T. K. McKenna, S. Menary, J. M. Michan, T. Momose, J. J. Munich, K. Olchanski, A. Olin, P. Pusa, C. Ø. Rasmussen, F. Robicheaux, R. L. Sacramento, M. Sameed, E. Sarid, D. M. Silveira, D. M. Starko, G. Stutter, C. So, T. D. Tharp, R. I. Thompson, D. P. van der Werf, and J. S. Wurtele, *Nature* **561**, 211 (2018).
- [6] N. Masuhara, J. M. Doyle, J. C. Sandberg, D. Kleppner, T. J. Greytak, H. F. Hess, and G. P. Kochanski, *Phys. Rev. Lett.* **61**, 935 (1988).
- [7] G. Gabrielse, B. Glowacz, D. Grzonka, C. D. Hamley, E. A. Hessels, N. Jones, G. Khatri, S. A. Lee, C. Meisenhelder, T. Morrison, E. Nottet, C. Rasor, S. Ronald, T. Skinner, C. H. Storry, E. Tardiff, D. Yost, D. M. Zambano, and M. Zielinski, *Opt. Lett.* **43**, 2905 (2018).
- [8] K. S. E. Eikema, J. Walz, and T. W. Hänsch, *Phys. Rev. Lett.* **86**, 5679 (2001).
- [9] I. D. Setija, H. G. C. Werij, O. J. Luiten, M. W. Reynolds, T. W. Hijmans, and J. T. M. Walraven, *Phys. Rev. Lett.* **70**, 2257 (1993).
- [10] S. Wu, R. C. Brown, W. D. Phillips, and J. V. Porto, *Phys. Rev. Lett.* **106**, 213001 (2011).
- [11] L. De Marco, G. Valtolina, K. Matsuda, W. G. Tobias, J. P. Covey, and J. Ye, [arXiv:1808.00028](https://arxiv.org/abs/1808.00028) (2018).
- [12] B. K. Stuhl, B. C. Sawyer, D. Wang, and J. Ye, *Phys. Rev. Lett.* **101**, 243002 (2008).
- [13] J. F. Barry, D. J. McCarron, E. B. Norrgard, M. H. Steinecker, and D. DeMille, *Nature* **512**, 286 (2014).
- [14] L. Anderegg, B. L. Augenbraun, E. Chae, B. Hemmerling, N. R. Hutzler, A. Ravi, A. Collopy, J. Ye, W. Ketterle, and J. M. Doyle, *Phys. Rev. Lett.* **119** (2017).
- [15] S. Truppe, H. J. Williams, M. Hambach, L. Caldwell, N. J. Fitch, E. A. Hinds, B. E. Sauer, and M. R. Tarbutt,

- Nat. Phys. **13**, 1173 (2017).
- [16] A. L. Collopy, S. Ding, Y. Wu, I. A. Finneran, L. Anderegg, B. L. Augenbraun, J. M. Doyle, and J. Ye, [arXiv:1808.01067](#) (2018).
 - [17] M. S. Safronova, D. Budker, D. DeMille, D. F. J. Kimball, A. Derevianko, and C. W. Clark, [Rev. Mod. Phys.](#) **90**, 025008 (2017).
 - [18] D. DeMille, [Phys. Today](#) **68**, 34 (2015).
 - [19] J.-P. Uzan, [Rev. Mod. Phys.](#) **75**, 403 (2003).
 - [20] I. Kozryyev and N. R. Hutzler, [Phys. Rev. Lett.](#) **119**, 133002 (2017).
 - [21] S. K. Tokunaga, C. Stoeffler, F. Auguste, A. Shelkownikov, C. Daussy, A. Amy-Klein, C. Chardonnet, and B. Darquié, [Mol. Phys.](#) **111**, 2363 (2013).
 - [22] S. B. Cahn, J. Ammon, E. Kirilov, Y. V. Gurevich, D. Murphree, R. Paolino, D. A. Rahmlow, M. G. Kozlov, and D. DeMille, [Phys. Rev. Lett.](#) **112**, 163002 (2014).
 - [23] J. J. Hudson, D. M. Kara, I. J. Smallman, B. E. Sauer, M. R. Tarbutt, and E. A. Hinds, [Nature](#) **473**, 493 (2011).
 - [24] J. Baron, W. C. Campbell, D. DeMille, J. M. Doyle, G. Gabrielse, Y. V. Gurevich, P. W. Hess, N. R. Hutzler, E. Kirilov, I. Kozryyev, B. R. O’Leary, C. D. Panda, M. F. Parsons, E. S. Petrik, B. Spaun, A. C. Vutha, and A. D. West (ACME Collaboration), [Science](#) **343**, 269 (2013).
 - [25] W. B. Cairncross, D. N. Gresh, M. Grau, K. C. Cossel, T. S. Roussy, Y. Ni, Y. Zhou, J. Ye, and E. A. Cornell, [Phys. Rev. Lett.](#) **119**, 153001 (2017).
 - [26] J. Söding, R. Grimm, Y. B. Ovchinnikov, P. Bouyer, and C. Salomon, [Phys. Rev. Lett.](#) **78**, 1420 (1997).
 - [27] X. Miao, E. Wertz, M. G. Cohen, and H. Metcalf, [Phys. Rev. A](#) **75**, 011402 (2007).
 - [28] M. A. Norcia, J. R. K. Cline, J. P. Bartolotta, M. J. Holland, and J. K. Thompson, [New J. Phys.](#) **20**, 023021 (2018).
 - [29] J. Dalibard and C. Cohen-Tannoudji, [J. Opt. Soc. Am. B](#) **6**, 2023 (1989).
 - [30] P. D. Lett, R. N. Watts, C. I. Westbrook, W. D. Phillips, P. L. Gould, and H. J. Metcalf, [Phys. Rev. Lett.](#) **61**, 169 (1988).
 - [31] N. J. Fitch and M. R. Tarbutt, [ChemPhysChem](#) **17**, 3609 (2016).
 - [32] S. D. Hogan and F. Merkt, [Phys. Rev. Lett.](#) **100**, 043001 (2008).
 - [33] S. D. Hogan, C. Seiler, and F. Merkt, [Phys. Rev. Lett.](#) **103**, 123001 (2009).
 - [34] R. Taïeb, R. Dum, J. I. Cirac, P. Marte, and P. Zoller, [Phys. Rev. A](#) **49**, 4876 (1994).
 - [35] V. V. Ivanov and S. Gupta, [Phys. Rev. A](#) **84**, 063417 (2011).
 - [36] V. V. Ivanov, [Opt. Commun.](#) **324**, 258 (2014).
 - [37] S. Bennetts, C.-C. Chen, B. Pasquiou, and F. Schreck, [Phys. Rev. Lett.](#) **119**, 223202 (2017).
 - [38] In preparation.
 - [39] See Supplemental Material.
 - [40] W. D. Phillips and H. Metcalf, [Phys. Rev. Lett.](#) **48**, 596 (1982).
 - [41] M. Ben Dahan, E. Peik, J. Reichel, Y. Castin, and C. Salomon, [Phys. Rev. Lett.](#) **76**, 4508 (1996).
 - [42] S. R. Wilkinson, C. F. Bharucha, K. W. Madison, Q. Niu, and M. G. Raizen, [Phys. Rev. Lett.](#) **76**, 4512 (1996).
 - [43] T. P. Dinneen, K. R. Vogel, E. Arimondo, J. L. Hall, and A. Gallagher, [Phys. Rev. A](#) **59**, 1216 (1999).
 - [44] A. Cooper, J. P. Covey, I. S. Madjarov, S. G. Porsev, M. S. Safronova, and M. Endres, [arXiv:1810.06537](#) (2018).
 - [45] M. S. Safronova, S. G. Porsev, U. I. Safronova, M. G. Kozlov, and C. W. Clark, [Phys. Rev. A](#) **87**, 012509 (2013).
 - [46] T. Nicholson, S. Campbell, R. Hutson, G. Marti, B. Bloom, R. McNally, W. Zhang, M. Barrett, M. Safronova, G. Strouse, W. Tew, and J. Ye, [Nat. Commun.](#) **6**, 6896 (2015).

SUPPLEMENTAL MATERIAL

Sisyphus Optical Lattice Accelerator

The SOLD deceleration scheme brings atoms ultimately to zero mean velocity in the reference frame of the lattice. By applying a small frequency difference between two lattice beams, a lattice will move at a well-controlled speed [41, 42]. This implies that the SOLD can ideally decelerate or accelerate atoms to any desired velocity. We test this using a 1.53(2) μK stationary cloud produced by loading a MOT into a dipole trap, at the location of the lattice. We shine both lattice and pumping light onto this cloud for 100 μs and after 20 ms observe the number of atoms in a displaced cloud corresponding to the moving lattice frame. The results are shown in Fig. 6. We observe an increase in the displaced fraction with lattice height, which we attribute to the increase in energy $\sim U_{\text{lat}}/2$ given to the atoms for each scattering event. We also observe an optimal lattice velocity for a given lattice height, which roughly corresponds to our model criterion of eq. 1 with $m = 1$. The variation in the location of these efficiency peaks is more visible in Fig. 6 than in Fig. 3, because here the SOLD is pulsed for a short duration instead of operating in the steady-state regime, so the effects of the resonances corresponding to Eq. 1 are more pronounced.

We can also use the moving lattice to characterize our reservoir dipole trap. The loading of this reservoir is both sensitive to the mean velocity of atoms and to the location they end up when reaching zero mean velocity. We characterize the velocity acceptance of the reservoir by varying the frequency difference between the two lattice beams. The loading efficiency of the reservoir depending on the lattice velocity is shown in Fig. 7. It can be fitted by a Gaussian whose width is $\sigma_v = 0.0084(4) \text{ m.s}^{-1}$, centered at $v_R \sim -0.002 \text{ m.s}^{-1}$. This slight departure from zero velocity can be explained by the orientation of the reservoir relative to the guide, which favors the loading of atoms that move backward. We include this measured velocity selectivity of the reservoir in our model of the SOLD.

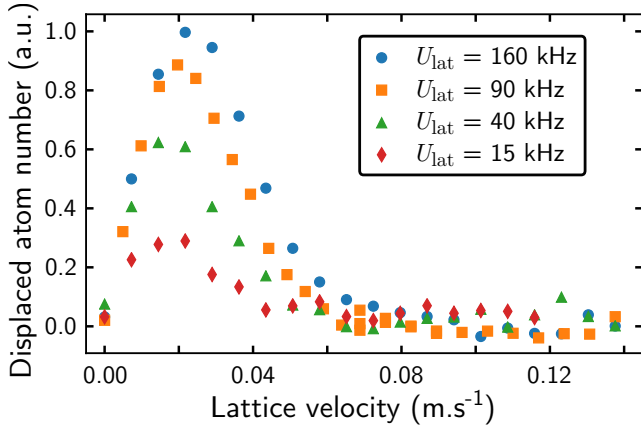


Figure 6. Acceleration of a stationary strontium cloud by a moving lattice, for various lattice heights. The abscissa gives the lattice velocity and the ordinate is proportional to the fraction of atoms in the moving frame measured after 100 μ s of acceleration followed by 20 ms of evolution.

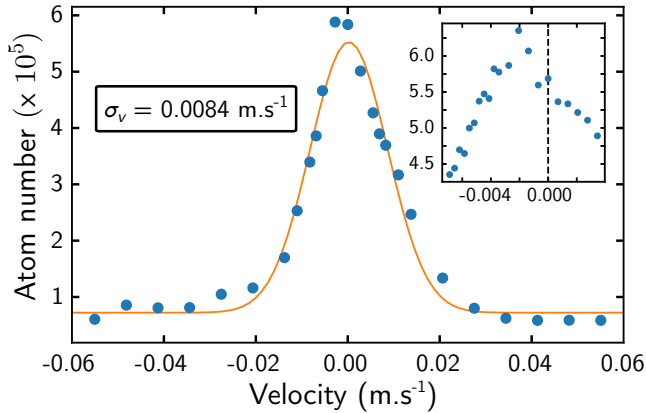


Figure 7. Velocity selectivity of the reservoir loading, measured by varying the lattice velocity. The line is a Gaussian fit of the data with width σ_v . The inset shows the same type of measurement on a much narrower velocity range, highlighting the center velocity of about $v_R \sim -0.002 \text{ m.s}^{-1}$.

SOLD Model

Here we give a description of our model of the SOLD that is an extended version of the description given in the main text.

In order to model our cooling scheme in an insightful way, we split the problem into two parts: the average energy lost per cooling cycle and the pumping rate. We then use both results to simulate the time evolution of the atoms' velocity.

Energy lost

We begin with a study of the energy lost due to the presence of the lattice. We assume that the atoms are optically pumped into the $^3\text{P}_1$ state at the bottom of

the lattice and we solve the differential equation for the motion $z(t)$ along the lattice propagation axis:

$$\frac{1}{2}mv_0^2 = U_{\text{lat}} \sin^2 k_{\text{lat}} z + \frac{1}{2}m \left(\frac{dz}{dt} \right)^2, \quad z(t=0) = 0, \quad (2)$$

with m and v_0 being respectively the mass and the initial velocity of the atom. U_{lat} is the lattice depth and $k_{\text{lat}} = \frac{2\pi}{\lambda_{\text{lat}}}$ is the wave vector of the lattice light with wavelength λ_{lat} . The solution of this equation can be written in terms of the Jacobi amplitude J_A :

$$z(t) = \frac{1}{k_{\text{lat}}} J_A \left(k_{\text{lat}} v_0 t, \frac{2U_{\text{lat}}}{mv_0^2} \right). \quad (3)$$

Since the process relies on spontaneous emission towards $^1\text{S}_0$, we determine the average energy lost $E_{\text{lost}}(U_{\text{lat}}, v_0)$ by integrating the lattice height explored for a duration set by the natural linewidth Γ of the $^1\text{S}_0 - ^3\text{P}_1$ transition,

$$E_{\text{lost}} = \Gamma \int_0^\infty e^{-\Gamma t} U_{\text{lat}} \sin^2(k_{\text{lat}} z(t)) dt. \quad (4)$$

In Fig 4(a), we show the evolution of E_{lost} for several lattice heights and depending on the incoming velocity. We observe that for high incoming kinetic energies compared to the lattice height $\frac{1}{2}mv_0^2 \gg U_{\text{lat}}$, the energy lost E_{lost} saturates. In this case, atoms travel through several lattice sites, and their propagation tends to $z(t) \rightarrow \frac{1}{k_{\text{lat}}} J_A(k_{\text{lat}} v_0 t, 0) = v_0 t$. Equation (4) gives the relation $E_{\text{lost}} \rightarrow \frac{U_{\text{lat}}}{2} / \left(1 + \left(\frac{\Gamma}{2k_{\text{lat}} v_0} \right)^2 \right)$.

In our experiment $v_0 \gg \lambda_{\text{lat}} \Gamma$, so the average energy lost saturates to $U_{\text{lat}}/2$. One striking feature of Fig 4(a) is that the energy lost exhibits a sharp resonance for $\frac{1}{2}mv_0^2 = U_{\text{lat}}$, where cooling is the most efficient. In this case, atoms have just enough energy to climb on top of the first lattice hill, so they spend most of their time at this location, which makes them more likely to spontaneously emit there and therefore to lose most of their kinetic energy. Indeed, the explored lattice height becomes $U(t) \rightarrow U_{\text{lat}} \tanh^2(k_{\text{lat}} v_0 t)$, which for $v_0 \gg \lambda_{\text{lat}} \Gamma$ gives an average energy lost reaching asymptotically $E_{\text{lost}} \rightarrow U_{\text{lat}}$.

Pumping rate

We now examine the pumping rate in dependence of the incoming velocity and lattice height. We solve the optical Bloch equation for a two-level system corresponding to the $^1\text{S}_0$ and $^3\text{P}_1$ states, coupled by the pumping laser with Rabi frequency Ω . The time-dependent Schrödinger - von Neumann equation for the density operator ρ is

$$\frac{d\rho}{dt} = -\frac{i}{\hbar} [H, \rho] + L, \quad (5)$$

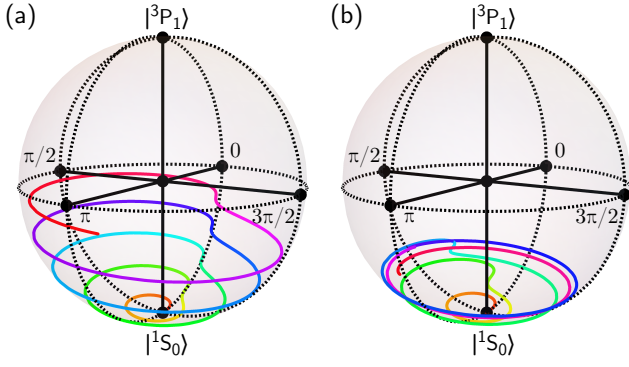


Figure 8. Evolution of the Bloch vector on the Poincaré sphere, shortly after the application of the SOLD. Atoms begin in the 1S_0 state at the location of a lattice site. The saturation parameter of the pumping to 3P_1 is set for clarity to about 60, and the lattice height is $h \times 600$ kHz. The velocity in (a) $v_0 = 0.1035 \text{ m.s}^{-1}$ is such that the accumulated phase during the travel time between two sites is close to $\Phi = 2\pi$, while in (b) where $v_0 = 0.09 \text{ m.s}^{-1}$ this condition is not met.

with \hbar the reduced Planck constant, L the usual term to account for the spontaneous emission due to Γ , and with the Hamiltonian H written as:

$$H = \begin{pmatrix} 0 & \Omega/2 \\ \Omega/2 & U_{\text{lat}} \sin^2(k_{\text{lat}} v_0 t) \end{pmatrix}. \quad (6)$$

We numerically solve equation 5 with time, starting with all the population in 1S_0 at $t = 0$. For this calculation, we assume a constant velocity v_0 , which is valid for $\frac{1}{2}mv_0^2 \gg U_{\text{lat}}$. After a variable time, the $(\Omega, U_{\text{lat}}, v_0)$ -dependent solution for the excited population reaches a steady-state only slightly perturbed by the time-dependent detuning produced by travelling within the lattice. Averaging over this small perturbation, we get the population in the 3P_1 state shown in Fig. 5.

The remarkable feature in this figure is the presence of sharp lines where the excited population is the highest. These can be simply explained by looking at the evolution of the Bloch vector associated with ρ , displayed in Fig. 8. When the atoms are not located at the bottom of a lattice site, the detuning is so strong that effectively the scattering rate vanishes, so the population distribution remains roughly constant for timescales short relative to Γ . Due to the dephasing between both states, the Bloch vector then evolves mainly horizontally, until the atoms reach the location of the bottom of the next lattice site. If at that moment the dephasing amounts to a multiple of 2π , then the effective pumping pulses add constructively, and the steady-state excited population is high. This leads to the resonance lines in Fig. 5.

We can give a simple quantitative criterion for the positions of these lines. The phase accumulated during the propagation through one lattice period is $\Phi = \Delta T$, with $T = \frac{\lambda_{\text{lat}}}{2v_0}$ the propagation time and Δ the dephasing, taken as the average detuning due to the lattice, giving $\Delta = 2\pi \frac{1}{h} \frac{U_{\text{lat}}}{2}$, with h the Planck constant. The condi-

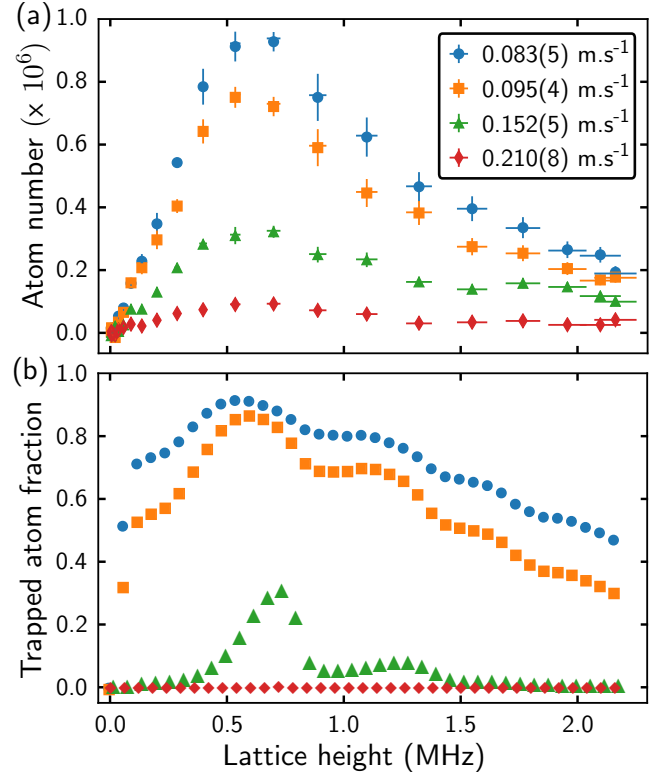


Figure 9. Comparison between (a) the experimental data already shown in Fig. 3 and (b) the results of the theoretical model (see text) for the same initial mean velocities.

tion $\Phi = m \times 2\pi$ (with $m \in \mathbb{N}$) gives the relation:

$$\frac{U_{\text{lat}}}{h} = m \times \frac{4v_0}{\lambda_{\text{lat}}}. \quad (7)$$

This criterion is shown as dashed red lines for $m \in \{1, \dots, 7\}$ in Fig 5.

Overall evolution

In order to model the complete behavior of the SOLD, we solve classically the evolution of the atoms' velocity v with time, under an effective force $F(U_{\text{lat}}, v) = -\Gamma \times \rho_{^3P_1}(U_{\text{lat}}, v) E_{\text{lost}}(U_{\text{lat}}, v)$. We carry out this calculation for a packet of atoms whose velocity distribution follows a (1D) Boltzmann distribution corresponding to the temperature of our MOT of $6 \mu\text{K}$ summed with an offset corresponding to the measured mean velocity given by the launch beam. The capture probability in our reservoir is determined by the velocity-dependent efficiency extracted from the measurement shown in Fig. 7, corresponding to a Gaussian function with a width $\sigma_v = 0.0084 \text{ m.s}^{-1}$. We thus simulate the time evolution of the loaded population in the reservoir depending on the lattice height, for the four mean starting velocities shown in Fig. 3. In Fig. 9 we compare the results from this model with our experimental data.

We see a good qualitative agreement concerning the overall behavior with both lattice height and starting mean velocity. In particular, the locations of the maximums of loading efficiency are well reproduced by our model. These correspond to the case when the starting mean velocity v_0 verifies the criterion of eq. 1 (with $m = 1$). Indeed, in that case atoms are efficiently pumped to the 3P_1 state, and lose typically a significant amount of energy $U_{\text{lat}}/2$. After spontaneous emission, their velocity is much lower and atoms are in the (U_{lat}, v) region where the density of lines for $m \geq 2$ is high. They are therefore very likely to keep decelerating efficiently. On the contrary, for high velocity v_0 , in the region $0 \ll \frac{U_{\text{lat}}}{h} \ll \frac{4v_0}{\lambda_{\text{lat}}}$, atoms will not get pumped to 3P_1 . Our model is thus able to estimate the capture velocity v_c of the SOLD, which is given by

$$v_c = \frac{U_{\text{lat}} \lambda_{\text{lat}}}{4h}. \quad (8)$$

Let us note that our model makes several approximations. Indeed the results of the calculations shown in Fig. 9(b) are given for one particular evolution time $t = 1.4$ ms that has been chosen for best match with the steady-state experimental data. Since no decay mechanism has been added in the model, the final loading would be with unity efficiency. This chosen deceleration time is rather short, because in this case the saturation parameter of the $^1S_0 - ^3P_1$ transition is set to ~ 320 , for which the calculations suffer less numerical errors compared to more realistic, lower saturation parameters. Nonetheless, the theory always exhibits the same overall behavior no matter the value of the saturation parameter. Another limitation of our model is that no selection criteria have been chosen for the position of atoms, whereas they must be in the vicinity of the crossing between the transport guide and reservoir to be loaded. Similarly, atoms expelled from the guide by the barrier formed by the blue detuned lattice and the effects of the lattice's slight angle with the guide are not taken into account. Finally, the constant velocity approximation made when solving the optical Bloch equations is not valid for $\frac{1}{2}mv_0^2 \leq U_{\text{lat}}$. To obtain a better quantitative agreement, Monte-Carlo simulations could be a straightforward option for further studies.

Atomic beam velocities

In order to characterize the dependence of the SOLD efficiency with incoming atom velocity, we need a measurement of the mean atom velocity within the transport guide before entering the lattice region. In the absence of the SOLD, we will assume the mean velocity to be constant throughout the lattice region, as the potential provided by the transport guide in this location is engineered to be flat in the axial direction.

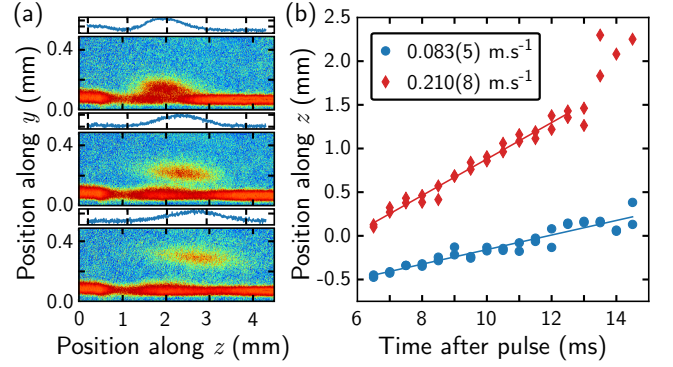


Figure 10. Measure of the atom beam velocity. (a) Absorption images and respective density profiles of clouds of atoms ejected from the transport guide, taken 5 ms (top), 8 ms (middle) and 10 ms (bottom) after the ejection pulse. The pulse is applied at $z \approx 1$ mm. (b) Evolution of the position along the z axis of two ejected clouds with different mean velocities. The lines are fits from which we extract the velocities.

We measure the atom velocity arriving at the location of the lattice by two methods. The first is to eject a burst of atoms out of the transport guide using a pulse of light resonant with the $^1S_0 - ^3P_1$ transition. The pulse lasts 1 ms and the laser beam propagates horizontally perpendicular to the atomic beam. We assume that spontaneously emitted photons are equally distributed in all directions during the ejection process, so that the on-axis mean velocity is not affected by the light absorption. By examining the propagation of the packet of ejected atoms, we can infer the mean velocity, see Fig. 10. We were only able to measure the mean velocity with high accuracy, as measurements of the axial distribution or temperatures of these ejected clouds were limited by low signal to noise. Rough estimates were however consistent with the measured MOT temperature of 6 μ K.

We use a second method as a cross-check for our determination of the atom mean velocity. It relies on the measurement of the loading in the transport guide region. Without the SOLD applied, we measure the steady-state atom number in the transport guide in the region corresponding to the extent of the lattice. We can extract the linear density ρ_{lin} in this region, if assumed to be homogeneous. By also assuming the mean velocity v_0 to be constant, we have the following relation for the steady-state incoming and outgoing flux:

$$F_{\text{lat,out}} = F_{\text{lat,in}} = \rho_{\text{lin}} \times v_0. \quad (9)$$

We thus need to measure $F_{\text{lat,out}} = F_{\text{lat,in}}$, which we get from the loading curves of the MOT and the transport guide. The rate equations for both MOT and transport guide atom numbers, N_{MOT} and N_{TG} , are

$$\begin{cases} \frac{dN_{\text{MOT}}}{dt} = F_{\text{in}} - \beta_{\text{TG,in}} N_{\text{MOT}} - \beta_{\text{MOT,loss}} N_{\text{MOT}} \\ \frac{dN_{\text{TG}}}{dt} = \eta_{\text{TG}} \beta_{\text{TG,in}} N_{\text{MOT}} - \beta_{\text{TG,out}} N_{\text{TG}} \end{cases}, \quad (10)$$

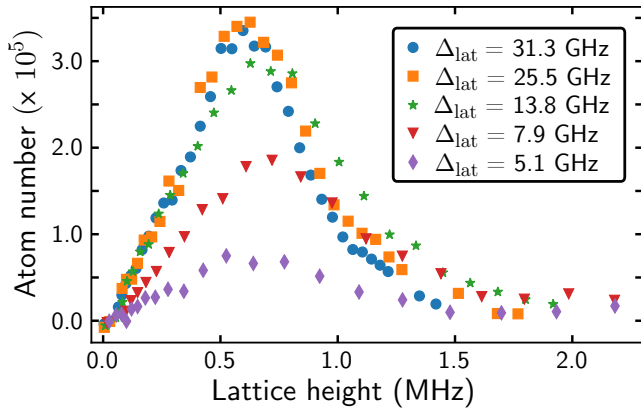


Figure 11. Effect of optical pumping by the lattice light to the 3S_1 state. The data shows the number of atoms loaded into the reservoir as a function of the lattice height for various detunings of the lattice laser from the $^3P_1 - ^3S_1$ transition.

where F_{in} is the flux coming into the MOT, see Ref. [37]. The loss rate $\beta_{\text{MOT,loss}}$ describes atoms lost from the MOT, while $\beta_{\text{TG,in}}$ describes the rate of atoms coupled into the beginning of the transport guide. The efficiency η_{TG} accounts for the losses between the start and the end of the guide. Last, the rate $\beta_{\text{TG,out}}$ describes atoms leaving the lattice region. We thus have $\beta_{\text{TG,out}} N_{\text{TG}}(t = \infty) = F_{\text{lat,out}} = F_{\text{lat,in}}$. From fitting the loading curves of both MOT and transport guide with the solutions of eq. 10, we extract the values of each β and η parameters, and ultimately get the value of v_0 . We found a good agreement between the velocities derived from both methods, and we use the first one to determine the values provided in the main text.

Losses toward 3S_1

One limitation of our decelerator is the optical pumping by the lattice light of atoms in the 3P_1 state to the 3S_1 state. If such optical pumping occurs, atoms can decay from 3S_1 to the metastable 3P_0 and 3P_2 states and exit the cooling cycle. Fig. 11 shows, for several lattice laser detunings Δ_{lat} , the effect of optical pumping to 3S_1 depending on the lattice height. For detunings a few GHz away from the $^3P_1 - ^3S_1$ transition we see a clear reduction of the atom number slowed and captured in the reservoir. For detunings above 20 GHz, the efficiency seems to converge toward a unique curve, indicating no significant optical pumping.

A repumping scheme such as the one used in Ref. [43] can optically pump atoms back to 3P_1 . Apart from a few additional photon recoils, this method should not significantly affect the slowing process, providing the repumping time is short compared to the propagation of the atoms along the lattice. Another simple method is to detune the lattice laser frequency further away from the $^3P_1 - ^3S_1$ transition, while adapting its power to keep

Table II. Relative uncertainties on the relevant parameters used to calculate the lattice height on the 3P_1 state.

	uncertainty
Lattice beam power P	$\pm 3.0\%$
Lattice beam waist w_0	$\pm 1.4\%$
Lattice frequency detuning Δ_{lat}	$\pm 0.1\%$
Total transition rate $A_{^3P_J - ^3S_1}$	$\pm 1.0\%$
Total uncertainty	$\pm 4.2\%$

the same lattice height. Aside from the data of Fig. 11, we operate at a lattice detuning of $\Delta_{\text{lat}} \approx 30$ GHz, for which optical pumping is negligible.

Lattice height determination

An accurate determination of the lattice height is essential for the characterization of the SOLD. The potential of a 1D lattice acting on the 3P_1 state is given by

$$U(z) = -\frac{1}{2\epsilon_0 c} \alpha_i I(z) = -\frac{4P}{\pi\epsilon_0 c w_0^2} \alpha_i \sin^2 k_{\text{lat}} z, \quad (11)$$

where α_i is the dynamic dipole polarizability of the 3P_1 state, P is the power of each lattice beam, and w_0 is their waist. In the two-level approximation,

$$\alpha_i \approx \frac{3\epsilon_0 \lambda_{\text{lat}}^3}{8\pi^2} \frac{\Gamma_{\text{eff}}}{\Delta_{\text{lat}}}, \quad (12)$$

where ϵ_0 is the vacuum permittivity. The approximation is valid because the lattice laser detuning Δ_{lat} is only a few tens of GHz. The effective rate $\Gamma_{\text{eff}} = \eta A_{^3P_1 - ^3S_1}$ is the effective transition rate for the $5s5p\ ^3P_1 - 5s6s\ ^3S_1$ transition, with $\eta = 1/2$ due to the lattice laser polarization. The relative uncertainties of the parameters contributing to the determination of the lattice height are listed in Tab. II. All parameters and their uncertainties are determined experimentally, except for the transition rate, which we derive from literature in the following manner.

The $^3P_J - ^3S_1$ manifold transition rates are known accurately to the percent level. In Ref. [45], *ab-initio* calculated matrix elements for the relevant contributing transitions, together with experimental transition energies, are used to evaluate the 3P_0 polarizability. Constraints from both the measurement of the magic wavelength at 813 nm and the dc polarizability are then imposed to fine-tune the dominant matrix element terms, in order to agree with the experimental values. The fine-tuning of these matrix elements does not exceed 1.1%, and the theoretical transition rate for $^3P_1 \rightarrow ^3D_1$ calculated from these matrix elements agrees with the measured value [46] to within 0.2%.

From the dipole matrix elements of $5s5p\ ^3P_0-5s6s\ ^3S_1$ calculated in Ref. [45], we determine the value of $A_{3P_1-3S_1}$. To this end, we calculate the branching ratios of the 3S_1 state to the three $5s5p\ ^3P_J$ fine structure states using Wigner 6-j symbols. We take into account the fine structure splitting of the states, which

is on the order of a few 100 cm^{-1} , and apply the frequency dependent correction factors to the branching ratios. The resulting branching ratios are from 3S_1 to $(^3P_0, ^3P_1, ^3P_2) = (12.02\%, 34.71\%, 53.27\%)$. Using these ratios, we derive the transition rate $A_{3P_1-3S_1} = 2.394(0.024) \times 10^7\text{ s}^{-1}$.